Focusing of therapeutic ultrasound through a human skull: A numerical study

Jie Sun and Kullervo Hynynen
Division of MRI/Department of Radiology, Brigham and Women's Hospital, Harvard Medical School, Boston, Massachusetts 02115

(Received 15 December 1997; revised 7 May 1998; accepted 2 June 1998)

A numerical model was developed which can use digitized layer interfaces to calculate ultrasound wave absorption, diffraction, reflection, and refraction. This model was used to evaluate the feasibility of ultrasound therapy and surgery through a human skull. A digitized human skull profile was obtained from magnetic resonance (MR) images and used to calculate the ultrasound field in the brain of a volunteer from a spherically curved phased array. With no phase correction, the focus of the array was shifted and defocused. The phased array technique was used to correct focal shift, reduce side lobes, and enhance focal amplitude. The optimum source element width was estimated for each frequency to obtain a near optimium focus, and an appropriate frequency range for transskull ultrasound therapy and surgery was determined. Acoustic pressure amplitude on the skull surfaces was examined, and it was shown that the skull heating problem could be overcome. Despite high attenuation, complex interface shape, and nonuniform thickness of a human skull, a sharply focused transskull ultrasound field can be generated for noninvasive ultrasound therapy and surgery in the brain. © *1998 Acoustical Society of America.* [S0001-4966(98)03709-6]

PACS numbers: 43.80.Sh, 43.35.Wa [FD]

INTRODUCTION

It has long been sought to use focused ultrasound to treat brain tumor,[1–11] and the skull has always been the biggest obstacle in the way. Until now, in order to use focused ultrasound for brain treatment, generally a piece of the skull has to be removed first. The removal of a piece of the skull is invasive, which significantly complicates the whole procedure. It is desirable to apply focused ultrasound through the intact skull; however, due to the skull's high sound speed (~2700 m/s), irregular shape and nonuniform thickness, it is practically impossible to obtain a sharp transskull focus at 1.0 MHz and above;[3,4,6,12] also due to skull's high attenuation, it is difficult to achieve enough focal amplitude without simultaneously overheating the skull.[3,11]

Phased arrays have been extensively studied and widely used in diagnostic medical ultrasound for several decades. By manipulating either or both amplitude and phase of the normal velocity specified at each source element, phased arrays can be used not only for conventional beam steering and spatial shading, but also for correction of ultrasonic beam degradation due to its propagation through inhomogeneous media. Smith *et al.* introduced this technique to ultrasound diagnostic imaging in order to correct the beam degradation due to the presence of intervening bone.[13,14] Thomas and Fink proposed to use this technique in therapeutic ultrasound, but only the results from a one-dimensional small element array were obtained.[15] Recently, it was demonstrated experimentally that it is practical to use two-dimensional large phased arrays for transskull ultrasound therapy and surgery.[12] In this experiment, a piece of formaldehyde fixed human skull was used, and through which sonications were performed and tissue destruction was induced in the exposed rabbit brain, *in vivo*.

Contingent with the experimental study,[12] it is the intent of this paper to evaluate theoretically the feasibility of generating a sharply focused ultrasound field through a human skull for therapeutic purposes. A numerical model was developed and used to study the appropriate frequency range and the optimum phased array element size. In order to evaluate the skull heating problem, the pressure gains (ratios of the focal pressure amplitudes compare to those on the skull surfaces) and the specific absorption rate (SAR) gains (ratios of the focal SARs compare to those on the skull surfaces) are studied, and methods to increase them are explored. With the development of a clinical MRI guided and monitored ultrasound system[16] which makes it possible to accurately deposit ultrasound energy deep in tissues, the stage has been set to further examine the possibility of totally noninvasive ultrasound therapy and surgery in the brain.

I. THEORY

The problem of interest is shown in Fig. 1. [The file MAMM002B.GIF for the skull diagram is obtained from: ftp://cnephia.bio.uottawa.ca/ftp/BIODIAC/ZOO/VERTEBRA/DIAGBW/.] Consider a spherically curved phased array that is in contact with multilayer media; the basic problem of interest is to evaluate the acoustic pressure field in the tissue layers in front of the array due to its specified normal velocity distribution. To address this problem, a numerical model has been developed. This model is based on techniques developed by Fan and Hynynen[17,18] that allows the irregular tissue layer interface to be taken into account in the simulation.

The pressure radiated by an arbitrary source, whose characteristic dimension is small in terms of the acoustic wavelength, is determined by its surface-averaged acceleration, or its volume acceleration, i.e., the surface integral of the normal acceleration. A source small in terms of the

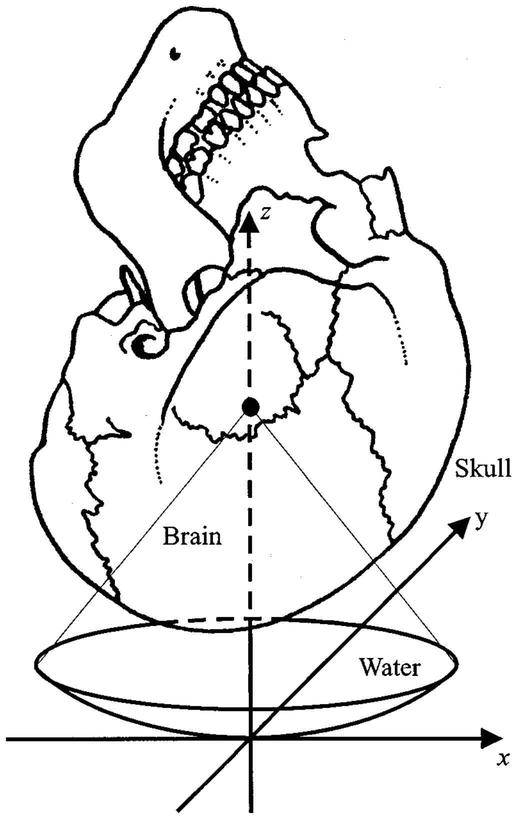

FIG. 1. The problem of interest.

acoustic wavelength can therefore be replaced by a point source (a simple source) embodying the same volume acceleration, regardless of the source geometry or of the local acceleration distribution over the source.[19]

A. Building block

Consider a small vibrating surface (area ds_1) in a medium. Its normal velocity u_1 can be specified if, e.g., it is on the surface of a transmitting transducer or caused by acoustic wave propagation. If the dimension of ds_1 is small enough compared with the acoustic wavelength, a simple source can be defined for the vibrating surface[19] with its source strength being denoted as $u_1\ ds_1$.

Assuming the simple source location is at (x_1,y_1,z_1), due to its baffled harmonic radiation, the corresponding acoustic pressure p at (x,y,z) can be written as[19,17]

$$p(x,y,z)=\frac{jk_{c_1}\rho_1 c_1}{2\pi}\frac{e^{-jk_{c_1}R}}{R}(u_1\ ds_1), \tag{1}$$

where $k_{c_1}=k-j\alpha_1$ is the complex wave number of the medium with α_1 being the attenuation coefficient, ρ_1 and c_1 are density and sound speed of the medium, respectively, and $R=\sqrt{(x-x_1)^2+(y-y_1)^2+(z-z_1)^2}$. Equation (1) is an alternative form of the classical Rayleigh–Somerfeld integral for a single simple source.

Now consider a small surface (area ds_2) at (x_2,y_2,z_2), and on different sides of which there are different media, i.e., ρ_1 and c_1 are density and sound speed of the first medium on one side, and ρ_2 and c_2 are density and sound speed of the second medium on the other side. The normal velocity of the surface due to the simple source $u_1\ ds_1$ can be written as[20,17]

$$u_2=\frac{jk_{c_1}}{2\pi}(u_1\ ds_1)\frac{e^{-jk_{c_1}R_{12}}}{R_{12}} \times\left(1-j\frac{1}{k_{c_1}R_{12}}\right)T_{v_2}\cos(\theta_{2t}), \tag{2}$$

where

$$R_{12}=\sqrt{(x_1-x_2)^2+(y_1-y_2)^2+(z_1-z_2)^2},$$

$$T_{v_2}=\frac{2}{(\rho_2 c_2/\rho_1 c_2)+[\cos(\theta_{2t})/\cos(\theta_{2i})]},$$

and θ_{2i}, θ_{2t} satisfy the Snell's law, i.e., $(\sin\theta_{2t}/\sin\theta_{2i})=c_2/c_1$. The effects of acoustic wave reflection and refraction are included in Eq. (2). Clearly, a new simple source can be defined at (x_2,y_2,z_2) with its source strength being denoted as $u_2\ ds_2$.

For a small vibrating surface, the pressure at the source location can be related to its normal velocity by a factor of the characteristic impedance of the medium right in front of the source,[21] e.g., for the sources above, the pressure at (x_l,y_l,z_l) can be approximated to be

$$p(x_l,y_l,z_l)=(\rho_l c_l)u_l, \tag{3}$$

where $l=1,2$. Equation (3) has been referred to as the impedance relation for linear plane waves.[22]

The equation relating the specific absorption rate (SAR) which is a descriptor of tissue heating and the pressure amplitude is also presented here for future reference,

$$\mathrm{SAR}=\alpha\frac{|p|^2}{\rho c}, \tag{4}$$

where $|p|$ is the pressure amplitude, α is the pressure attenuation coefficient, ρ and c are density and sound speed of the medium, respectively.

B. A multilayer problem

For a multilayer problem, an interface between adjacent layers will be divided into small pieces, and each piece will be treated as a simple source. A section of the layer interface which contains many simple sources can be considered as a secondary source.[20,17,23,24,18] Equation (2) can be used to relate the simple sources on one interface (which can be the transducer surface) to those on the next one, while Eq. (1) can be use to evaluate the acoustic pressure field in the last layer from the simple sources defined on the last layer interface. As stated before, the acoustic wave reflection and refraction at the layer interface are taken into account, but not the multiple reflection and reverberation in each layer.

Assuming $(M-1)$ tissue layers plus a layer (usually water) that is in direct contact with the transducer, the interface between layer l and $l+1$ is denoted the $(l+1)$th interface, while the first interface is actually the transmitting transducer surface. Subscript (or subsubscript) l will be used to denote the parameters on the lth interface, while index (or subscript) i will be used to denote the ith simple source, e.g., on the ith interface, there are N_l simple sources and the i_lth simple source, etc.

As an example, the equation for a two-layer problem is first presented. By combining Eqs. (1) and (2), the acoustic pressure in the second layer can be expressed as

$$
\begin{aligned}
p &= \sum_{i_2=1}^{N_2} \frac{jk_{c_2}\rho_2 c_2}{2\pi} \frac{e^{-jk_{c_2}R_{i_2}}}{R_{i_2}} (u_{i_2}\, ds_{i_2}) \\
&= \sum_{i_1=1}^{N_1} \sum_{i_2=1}^{N_2} \left[\frac{jk_{c_1}}{2\pi} \frac{e^{-jk_{c_1}R_{i_1,i_2}}}{R_{i_1,i_2}} \left(1 - j\, \frac{1}{k_{c_1}R_{i_1,i_2}} \right) \right. \\
&\quad \left. \times T_{v_{i_2}} \cos(\theta_{i_2,t}) \right] \left[\frac{jk_{c_2}\rho_2 c_2}{2\pi} \frac{e^{-jk_{c_2}R_{i_2}}}{R_{i_2}} \right] u_{i_1} (ds_{i_1}\, ds_{i_2}),
\end{aligned}
\tag{5}
$$

where $k_{c_1} = k - j\alpha_1$, $k_{c_2} = k - j\alpha_2$ are the complex wave numbers of the first and second layer, respectively, with α_1 and α_2 being the corresponding attenuation coefficients. $(x_{i_1}, y_{i_1}, z_{i_1})$ is used to denote the location of a simple source on the transducer, while $(x_{i_2}, y_{i_2}, z_{i_2})$ is used to denote the location of a simple source on the layer interface between the first and second layers.

$$R_{i_1,i_2} = \sqrt{(x_{i_1}-x_{i_2})^2 + (y_{i_1}-y_{i_2})^2 + (z_{i_1}-z_{i_2})^2}$$

and

$$R_{i_2} = \sqrt{(x-x_{i_2})^2 + (y-y_{i_2})^2 + (z-z_{i_2})^2}.$$

Apparently, summation over all the simple sources is an equivalent representation to integration over the transducer surface and the secondary source surface.

It is noted that

(1) In Eq. (5), the summations over the transducer surface and the secondary source surface are interchangeable, i.e.,

(a) By summing over the transducer surface first, the normal particle velocity at each simple source on the layer interface due to the whole transducer can first be obtained, then by summing over the whole secondary source surface, the total acoustic pressure can be obtained; or

(b) By summing over the secondary source surface first, the acoustic pressure due to each simple source on the transducer can first be obtained, then by summing up the acoustic pressure due to each simple source on the transducer, the total acoustic pressure can be obtained.

(2) Equation (5) can easily be extended to a multilayer problem by cascading layers using Eq. (2), e.g., for an M-layer problem, the pressure in the Mth layer can be expressed as

$$
\begin{aligned}
p = \overbrace{\sum_{i_1=1}^{N_1} \cdots \sum_{i_M=1}^{N_M}}^{M} \prod_{l=1}^{M-1} & \left[\frac{jk_{c_l}}{2\pi} \frac{e^{-jk_{c_l}R_{i_l,i_{l+1}}}}{R_{i_l,i_{l+1}}} \right. \\
& \left. \times \left(1 - j\, \frac{1}{k_{c_l}R_{i_l,i_{l+1}}} \right) T_{v_{i_{l+1}}} \cos(\theta_{i_{l+1},t}) \right] \\
& \times \left[\frac{jk_{c_M}\rho_M c_M}{2\pi} \frac{e^{-jk_{c_M}R_{i_M}}}{R_{i_M}} \right] u_{i_1} \left(\prod_{l=1}^{M} ds_{i_l} \right).
\end{aligned}
\tag{6}
$$

It is well known that the classical Rayleigh–Somerfeld integral is an expression of Huygen's principle which characterizes diffractive propagation as that of the linear sum of a field's constituent point sources;[25] obviously, Eq. (6) can be considered as an extended form of the Rayleigh–Somerfeld integral for a multilayer case.

(3) It is important to determine an effective secondary source area on the layer interface, so that outside this area, the simple source strength diminishes, i.e., the amplitude of normal particle velocity sharply decays at or inside the edge of the defined secondary source on the layer interface. Contrary to many other acoustic propagation problems, due to its narrow main beam, a secondary source area in front of a focused transducer can easily be determined to be confined in a reasonably small area.

(4) For the frequency range and typical transducer size of interest, the amount of the simple sources either on the transducer surface or on the secondary sources could be overwhelmingly large.

C. Digitized interface

For real human anatomies, e.g., a human skull, the layer interface has to come in the form of digitized data profiles. The numerical model is designed such that a data file with z coordinates over an equispaced rectangular x-y grid can be read in to specify the layer interface. Assuming the layer interface is continuous and so is its first order derivative, it is important to be able to calculate accurately the normal direction and area of a small piece on the layer interface which will be treated as a simple source.

A nine-point grid for $[x_{i-1}, x_i, x_{i+1}]$ and $[y_{j-1}, y_j, y_{j+1}]$ is extracted from the digitized layer interface which will be used to define a simple source at (x_i, y_j) in terms of its normal direction and area. Assuming the nine-point data are on a continuous surface specified by $z = f(x,y)$, for a tangential plane at $(x_i, y_j, f(x_i, y_j))$, its normal direction can be represented as $(f'_x(x_i,y_j), f'_y(x_i,y_j), -1)$, where $f'_x(x_i,y_j)$ and $f'_y(x_i,y_j)$ can be obtained approximately using the following Langrange formula,

$$
\begin{aligned}
f'_x(x_i,y_j) &= \frac{f(x_{i+1},y_j) - f(x_{i-1},y_j)}{x_{i+1} - x_{i-1}}; x_{i+1} > x_i > x_{i-1} \\
f'_y(x_i,y_j) &= \frac{f(x_i,y_{j+1}) - f(x_i,y_{j-1})}{y_{j+1} - y_{j-1}}; y_{j+1} > y_j > x_{j-1}.
\end{aligned}
\tag{7}
$$

Here, $f(x,y_j)$ is assumed to be continuous in $[x_{i-1},x_{i+1}]$ and $f(x_i,y)$ is assumed to be continuous in $[y_{j-1},y_{j+1}]$. This type of calculation is carried out for all the simple sources on a layer interface by simply moving the nine-point grid except at the edge of the layer interface profile where extrapolations are needed.

Assuming equal square area (dA) for the x-y plane projection of each simple source on the layer interface, the surface area for the simple source at (x_i,y_j) can be obtained as

$$ds=\frac{dA}{[\sqrt{(f_x'(x_i,y_j))^2+(f_y'(x_i,y_j))^2}]^{-1}}, \tag{8}$$

where the denominator is actually the corresponding directional cosine with respect to the z axis.

D. Phase correction

In a phased array architecture, the purpose of phase correction is to introduce extra phase offset to each source element so that the acoustic wave radiated from each source element will add up coherently at a desired focal point. The optimum case is that the radiated acoustic wave from each source element should arrive at the desired focal point with the same phase.

In the forward problem of evaluating the acoustic field radiated from a transducer, instead of integrating over the whole transducer surface at once, one can integrate over one element first and obtain its corresponding complex pressure at a desired focal point. With the complex pressure obtained, a phase delay can be calculated for the source element. Hence, phase delays can be obtained for all the source elements on a phased array, which will then be fed into the second iteration of the forward problem to obtain the acoustic field. If the integration in Eq. (6) is still performed for each source element separately, the complex pressure obtained at the desired focal point due to each source element should have the same phase. On the other hand, the phase-corrected acoustic field can be obtained by integrating over the whole transducer surface at once after feeding back the phase delay information for each source element.

When there are large amount of phased array elements, the procedure described above for calculating the phase delay for each source element can be a prohibitively tedious process. A second approach, the reversed problem, is devised. In the reversed problem, a point source is radiating at the desired focal point, and the complex pressure at each source element location on the transducer can be evaluated all at once, which will then be fed in to the forward problem.

II. SIMULATIONS

The numerical model was extensively tested before actually being used to evaluate the focused ultrasound field through a human skull.[26] A digitized human skull profile was built from MR images. Figure 2 shows the 3-D skull traces at different MR image slices for the skull's outer and inner surfaces, respectively. The benchmark configuration for our investigation is that a spherically curved transducer driven at 1.0 MHz; the transducer has a curvature radius of 10 cm and

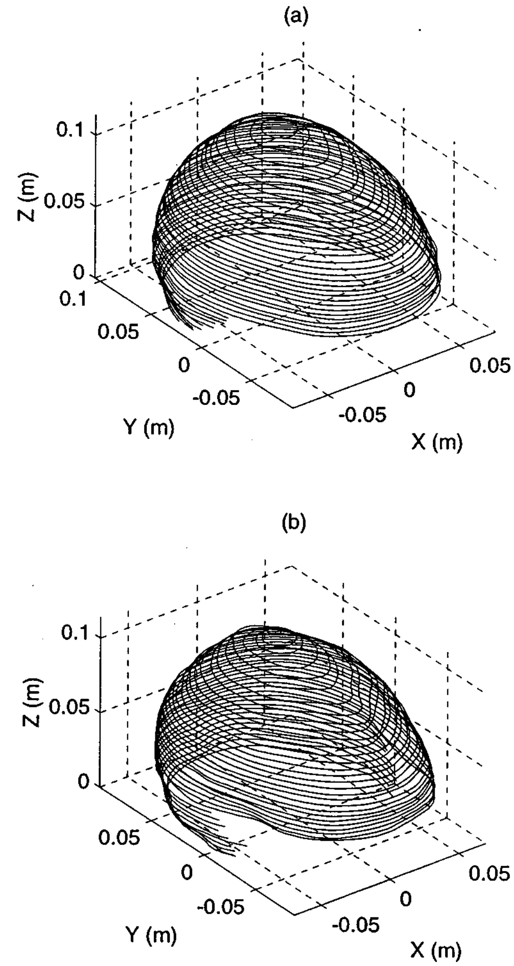

FIG. 2. A digitized human skull profile. Contours: (a) outer surface; (b) inner surface.

a diameter of also 10 cm (F number is 1.0); the transducer was positioned towards the skull such that the focal depth inside the skull was around 6 cm.

The phased array architecture is shown in Fig. 3 which is a two-dimensional diagram of the projection of an $M \times M$ element transducer (a 16×16 element transducer is shown in the figure, where M is chosen to be 16) in order to show how the phased array elements are divided. The projection is in the base plane of the transducer, i.e., in the x-y

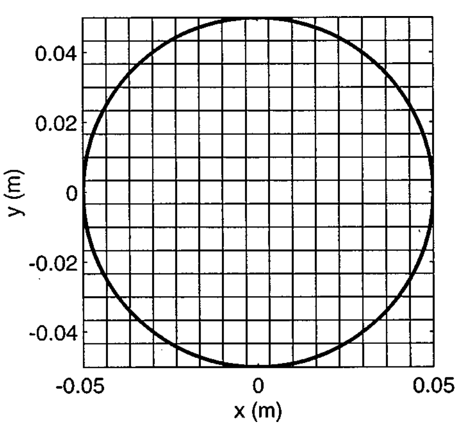

FIG. 3. Projection in the transducer base plane for the configuration of a 16×16 element phased array.

TABLE I. The properties of the three layers: the water–skull–brain layers in front of the transducer.

	Density (kg/m^3)	Sound speed (m/s)	Attenuation (nep/m) Frequency (MHz)								
			0.5	0.625	0.75	0.875	1.0	1.125	1.25	1.375	1.5
Water	998.0	1500					0.0				
Skull	1796.6	2652.6	50	50	85	137	179	223	315	390	464
Brain	1030.0	1545.0					4.0× frequency				

plane where $z=0.0$, clearly, the projection of each element has an equal square area, which will simply be referred to as a square element later on. It was shown that not all the $M \times M$ elements fall onto the transducer surface, some elements were outside the circular area of the transducer, hence the total number of source elements on the transducer was less than $M \times M$. However, for simplicity, if the width of a square element is obtained from dividing the diameter of the transducer by M, the corresponding phased array will still be referred as an $M \times M$ element transducer. The frequency range under investigation was from 0.5 to 1.5 MHz, with more details were presented for the 0.5-, 1.0-, and 1.5-MHz frequency cases. At 1.0 MHz, the effects of changing focal depth inside the skull from 1.0 to 8.0 cm were investigated, and a transducer with the same curvature radius but increased diameter of 13.625 cm (F number is 0.734) was also considered. The total acoustic power into the transducer was 1 W, so the following results can be interpreted as normalized quantities with a reference of 1-W total acoustic power, and the pressure and the normal velocity of interest due to some other total acoustic power can be scaled accordingly. The effects of nonlinear propagation can be ignored with this focused transducer as was shown by *in vivo* measurements.[27]

Although the skull is generally considered as bone, more detailed skull acoustic properties have to be taken into consideration. The acoustic properties of the human skull used in this paper are mainly derived according to a paper published by Fry and Barger.[4] The density and the sound speed of the skull were obtained by weighted averages combining inner table, diploe, and outer table. In the numerical model, the reflection loss has been taken into account, so the attenuation loss can be estimated by subtracting the reflection loss from the insertion loss. It has been shown that, in the human skull, the absorption loss is linearly proportional to the frequency, while the scattering loss is much more frequency dependent. Within the frequency range of 0.5–1.5 MHz, the scattering loss is a more dominant factor, particularly in diploe.[4] Table I shows the layer properties. A three-layer model was considered in front of the transducer, more specifically, water outside the skull, skull, and brain inside the skull. In the brain tissue, the attenuation is linearly related to the frequency, while in the skull, the attenuation is strongly dependent on the acoustic wave frequency.

The emphasis is on transskull ultrasonic field in the focal plane, while the axial ultrasonic field inside the brain is presented only for some examples. In order to have a better view of the acoustic field pattern, both surface and contour plots are presented, and the contour lines are drawn with the interval of 10% of the peak value.

III. RESULTS

Figure 4 shows the transskull ultrasonic field in the focal plane at 1.0 MHz. The 1×1 element case is presented as a reference, which is the uniform phased case with a single element. 4×4, 8×8, and 16×16 element cases are presented as examples to show the effects of phase correction. For 1×1 and 16×16 element cases, Fig. 5 shows the axial ultrasonic field in the brain also at 1.0 MHz, and the axial ultrasonic field is presented in the x-z and y-z planes that contain the focal point. Figure 6 shows the transskull ultrasonic field in the focal plane, for 1×1 and 16×16 element cases, at 0.5 and 1.5 MHz, respectively.

Figure 7 summarizes the change of the normalized focal amplitude versus the phased array element sizes (numbers). The ideal focal amplitudes were obtained with the 256×256 element phased array (total number of simple sources equals total number of source elements) which were used as normalization references. Three driving frequencies of 0.5, 1.0, and 1.5 MHz were considered. The focal amplitude increased with the increase of transducer element number (the decrease of the element size) at all frequencies. The focal amplitude approached the ideal value asymptotically and reached above 90% of the ideal value with element width of about 15 mm at 0.5 MHz, 10 mm at 1.0 MHz, and 6.7 mm at 1.5 MHz, respectively.

For real transskull therapy and surgery without skull overheating,[6,8,11] it is important to examine the relative pressure amplitude on the surface of and inside the skull compared with that at the focal point. As shown in Eq. (3), the pressure on the skull surfaces can be directly related to the normal velocity at the same point approximately. For the $F=1.0$ transducer, Fig. 8 shows the acoustic pressure amplitude on both the outer and inner surfaces of the skull for the 16×16 element case at 1.0 MHz. The acoustic pressure amplitude on the skull surface is presented in the coordinates that correspond to the x-y plane projection of the skull surface. From Fig. 8 and other simulations (not shown), it is clear that the pressure amplitude on the outer skull surface is larger than that on the inner skull surface. Table II summarizes the relative peak pressure amplitude on the skull surfaces compared with that at the focal point. A pressure gain is introduced as the ratio of the peak pressure amplitude at the focal point to that on the outer skull surface (ζ_o). In

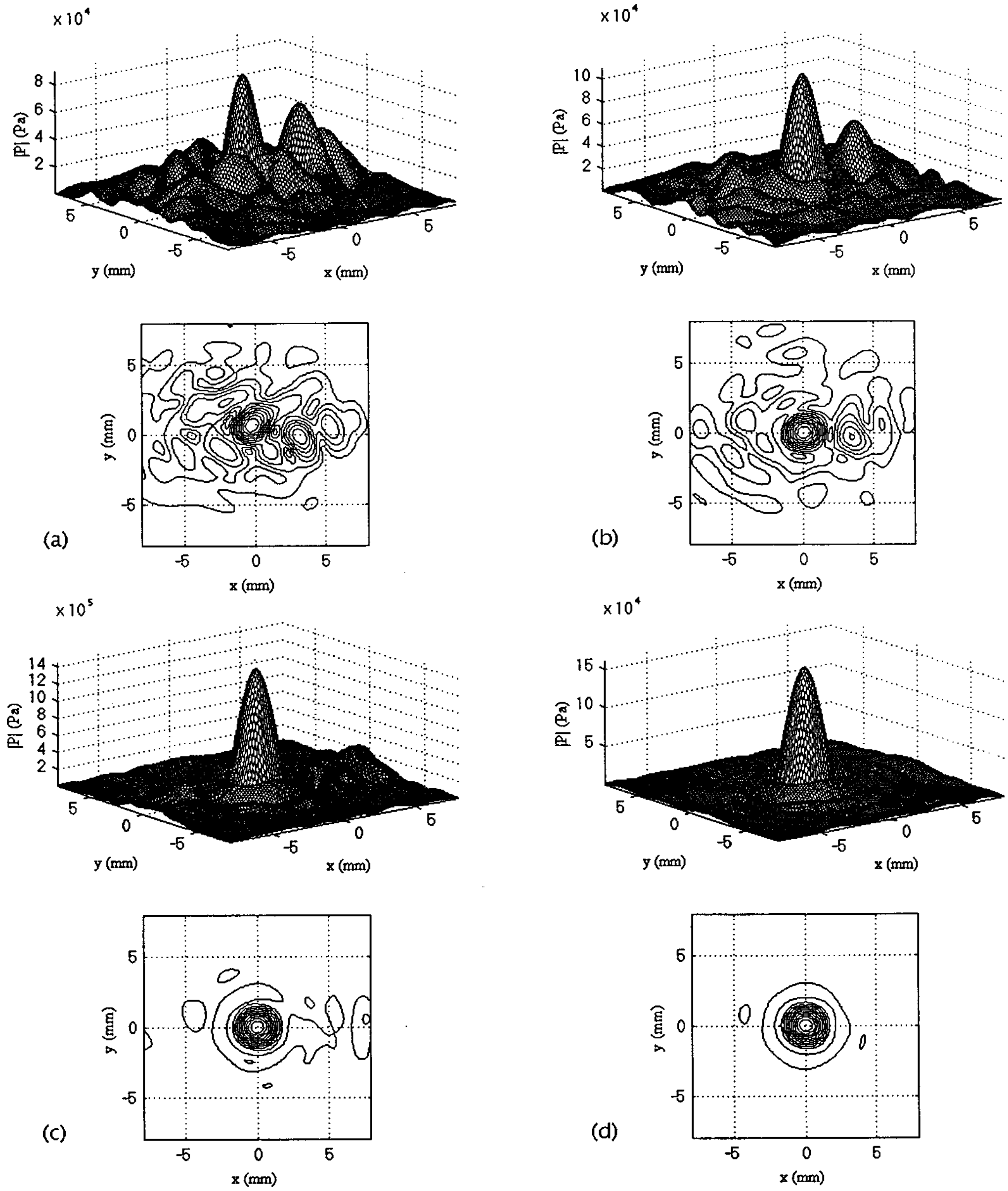

FIG. 4. The transskull ultrasonic field in the focal plane at 1.0 MHz: (a) 1×1; (b) 4×4; (c) 8×8; (d) 16×16.

order to ensure that no immediate skull heating adjacent to the brain which is a much worse case, the pressure gain of the peak pressure amplitude at the focal point compare to that on the inner skull surface (ζ_i) is also examined. Clearly, SAR gains can be similarly defined. To further investigate the frequency dependency of the pressure and SAR gains, a set of simulations were performed. Figure 9 shows both pressure and SAR gains as a function of frequency for the 16 ×16 element case. The pressure gain curve peaks at 0.60–0.65 MHz above which the value decays slowly and drops below 1.0 at about 1.25 MHz. The SAR gain curve shows very high value at low frequencies and quickly drops below 1.0 at about 0.85 MHz.

The influence of the focal depth inside the skull was also investigated, and the pressure and SAR gains are plotted in Fig. 10 for the 16×16 element case at 1.0 MHz. Both gains increase with the increase of focal depth.

IV. DISCUSSION

The simulation shows that it is possible to obtain a sharp focus through a human skull at a low frequency, or by using a phased array with phase correction. The pressure and SAR gains achieved show that transskull ultrasound therapy and surgery should be feasible with a single element spherically curved transducer at frequencies around 0.5 MHz, and with a phased array at frequencies up to 1.0 MHz. This agrees with the earlier experimental results.[12]

By using a single-element, spherically curved transducer, a sharp focus can be generated through the skull at frequencies up to 1.0 MHz, and the focus is destroyed by the phase shifts cause by the bone at higher frequencies. This agrees with many earlier works on single-element, spherically curved transducers.[3,6,12] By using a phased array with phase correction, the destroyed focus can be restored and a sharp focus can be generated through the skull. This is in

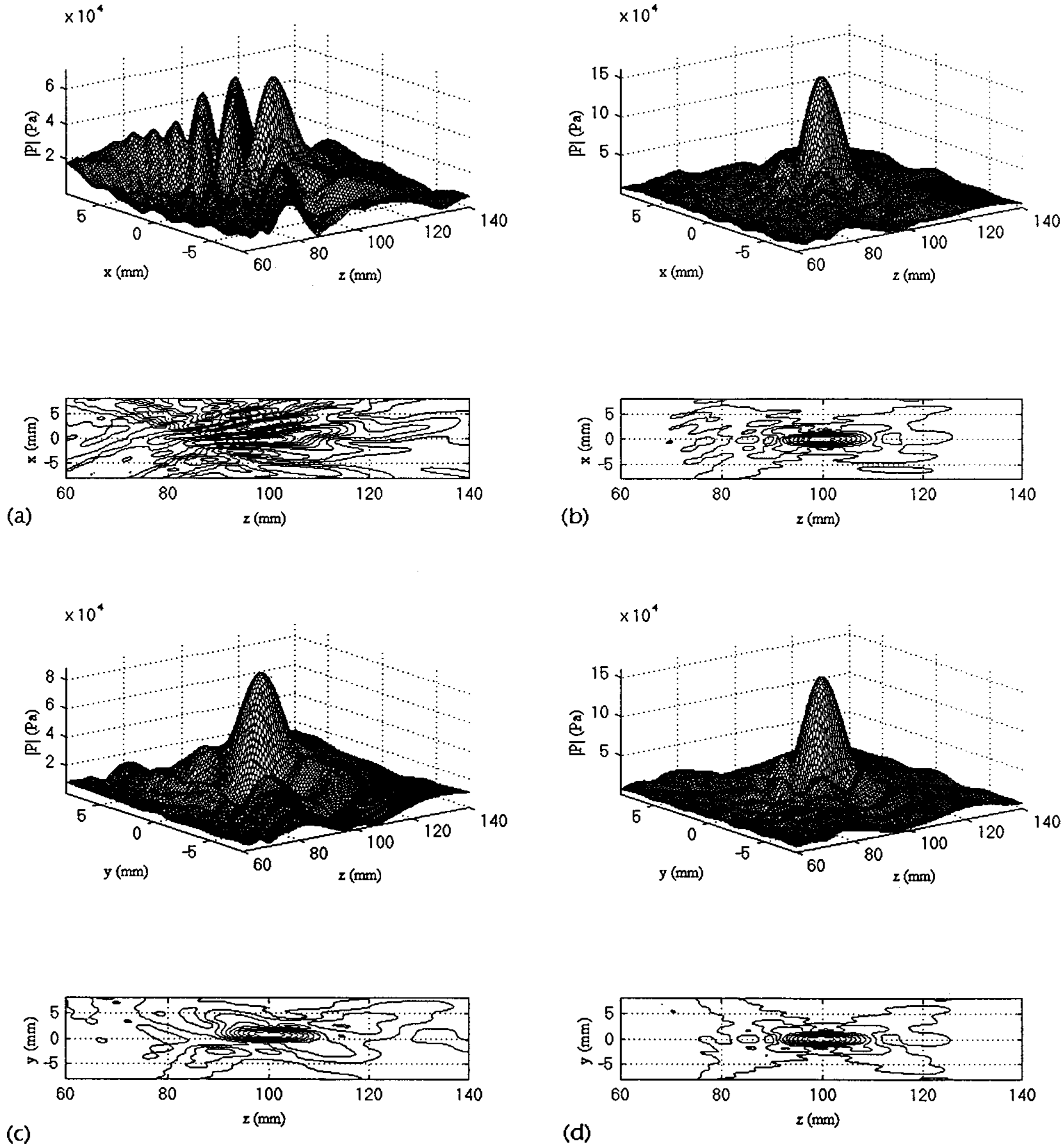

FIG. 5. The axial ultrasonic field in the brain at 1.0 MHz: (a) 1×1—in the axial *x*-*z* plane; (b) 16×16—in the axial *x*-*z* plane; (c) 1×1—in the axial *y*-*z* plane; (d) 16×16—in the axial *y*-*z* plane.

agreement with the one-dimensional array experiments[15] and the two-dimensional large array experiments.[12]

Both the single element and the phased array simulated field distribution show qualitatively the same fields as were detected experimentally,[12] which indicates that the numerical model is accurate enough for investigating the major physical parameters influencing the beam propagation through the skull.

At 1.0 MHz, without phase correction, the focus was shifted and the side lobes were unacceptable. The focal shift can be mostly corrected by using a 4×4 element phased array. The side lobes were further reduced and the focal amplitude was further enhanced by using more source elements. At 0.5 MHz, there was a clear dominant main lobe even without phase correction; the defocusing effect was not obvious, but the focus was clearly shifted. With a phased array, no significant increase of focal amplitude was observed, and the focal shift can be corrected by a 4×4 or more element phased array. At 1.5 MHz, the focus was totally destroyed without phase correction. With a 4×4 element phased array, the focus was restored at the desired location, but the side lobes were unacceptable. With more source elements, significant focal amplitude enhancement was achieved.

It is obvious that enhanced focal amplitude can be achieved by dividing the transducer into smaller elements (more elements); however, there is a limit, and a near optimum focus can be defined when the element is already small, in essence that there will be little or no focal amplitude improvement by using a smaller element size. From a practical point of view, smaller element size means more source elements and their corresponding hardware. The trade-off between the focal amplitude and the element size (number) has to be made. In Fig. 7, at 1.0 MHz (wavelength in water 1.5 mm), it is shown that an optimum focus can be obtained with a 10×10 element phased array (square element width 10.0 mm), i.e., when more source elements were used, little focal amplitude enhancement was achieved. Similarly, at 0.5 MHz (wavelength in water 3.0 mm), an optimum focus can be

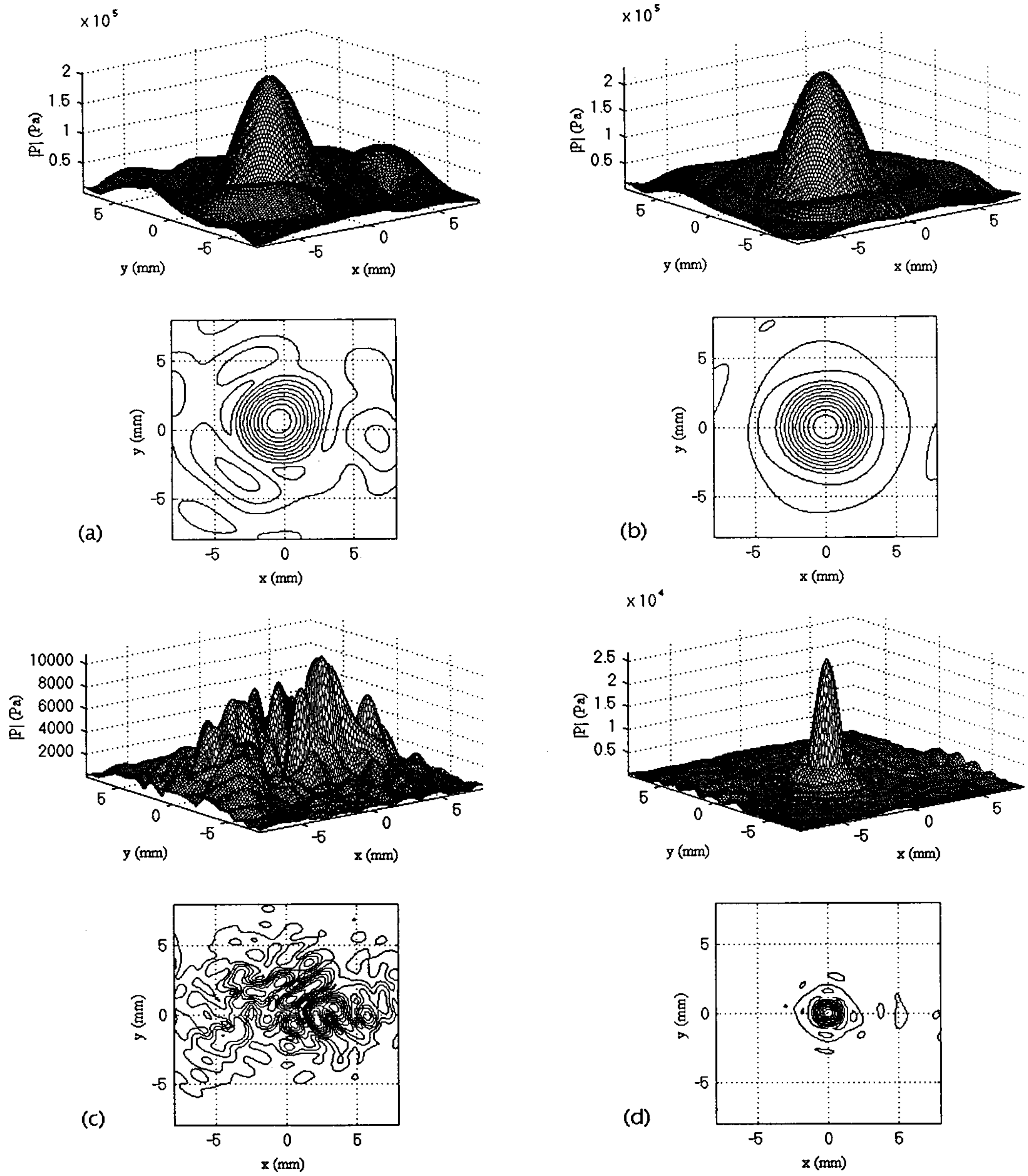

FIG. 6. The transskull ultrasonic field in the focal plane: (a) 1×1 at 0.5 MHz; (b) 16×16 at 0.5 MHz; (c) 1×1 at 1.5 MHz; (d) 16×16 at 1.5 MHz.

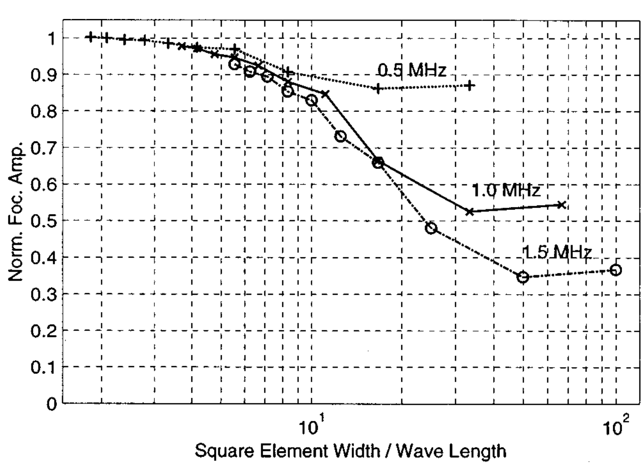

FIG. 7. Pressure/SAR gains versus the phased array element size.

obtained with a 6×6 element phased array (the square element width of ~16.7 mm), and at 1.5 MHz (wavelength in water 1.0 mm), an optimum focus can be obtained with a 14×14 element phased array (the square element width of ~7.1 mm). As a rule of thumb, in order to achieve a near optimum focus, the square element width should be less than 5–6 times the acoustic wavelength.

In Fig. 9, the pressure gain of as high as 4.5 has been observed, with the maximum observed SAR gain being about 3.1. It is apparent that, in order to deliver a predetermined amount of power deposition in the brain, the power flux through a unit area on the skull surface should be inversely proportional to penetration area. For the $F=1.0$ transducer, only about 1/6 of the available skull surface area is utilized. If the total available skull surface area were to be utilized, the peak pressure amplitude on the skull surfaces could be reduced by $1/\sqrt{6}$ assuming the same focal amplitude is maintained, hence the pressure gains could increase

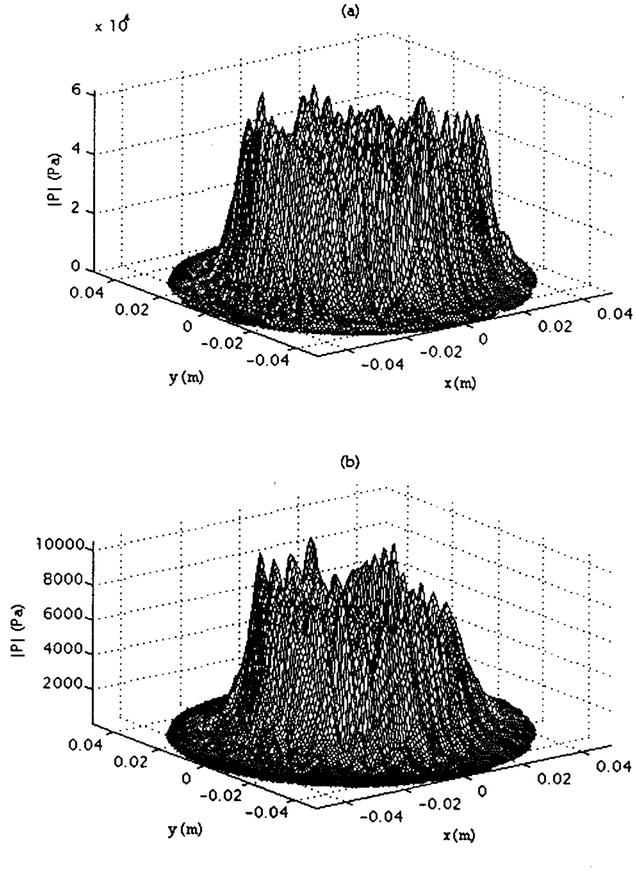

FIG. 8. The acoustic pressure amplitude on the skull surfaces for the 16 $\times$16 element case at 1.0 MHz: (a) outer surface; (b) inner surface.

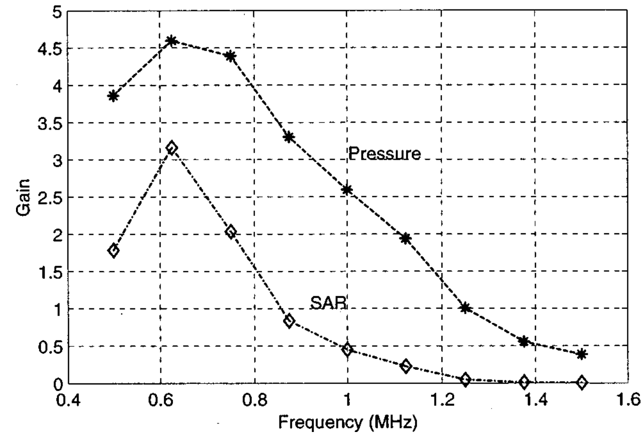

FIG. 9. Pressure/SAR gains versus frequency.

by $\sim\sqrt{6}$. The SAR gains could increase by 6.0, because the absorbed power is proportional to the pressure amplitude square. In order to avoid skull overheating, the SAR gains between the focal point and on the skull has to be larger than 1.0.[12] At 0.5–1.0 MHz, it might be possible to induce thermal effects in the brain for therapeutic purposes, and on the other hand, it has been demonstrated recently[12] that the cavitation effects might be another option, particularly for frequencies with only marginal achievable SAR gains. Although single location pulsed sonication appears to be controllable,[28] it is not known if the generated microbubbles would distort the power deposition when larger volumes are covered with multiple sonications. Clearly, much more works are needed before the cavitation mechanism can be used for brain therapy and surgery.

From Fig. 10, it is shown that the pressure gains are adequate only for relatively deep targets. If pressure gain of 1.5 is used as a guideline, the targets have to be deeper than 30.0 mm in the brain. On the other hand, it may be possible reach even more superficial targets when the whole skull surface is used for the transmission of the ultrasound beam. Similarly, it may be possible to treat superficial targets from the opposite side through the brain. However, this was not simulated here.

Despite the distortion caused by the presence of the skull, and the phase correction applied to correct and restore the focus, the linear relationship[29] between the focal volume (in terms of transverse focal width D_t, axial focal length D_a) and the acoustic wave frequency remains intact (Table II). Clearly, the focal volume is the largest at 0.5 MHz, and the

TABLE II. The peak acoustic pressure amplitude on the skull surface compared with that at the focal point.

		Peak pressure amplitude ($Pa\times10^3$)			Pressure gain		Focal dimensions (mm)	
	Frequency (MHz)	Focal point	Outer skull surface	Inner skull surface	ζ_o	ζ_i	D_t	D_a
1×1	0.5	202.8	55.2	27.2	3.7	7.5	3.0	20.0
	1.0 ($F=1.0$)	89.8	55.6	12.9	1.6	7.0	N/A	N/A
	1.0 ($F=0.734$)	102.8	38.1	12.2	2.7	8.4	N/A	N/A
	1.5	10.8	54.0	3.0	0.20	7.0	N/A	N/A
16×16	0.5	232.7	60.3	24.4	3.9	9.5	3.0	20.0
	1.0 ($F=1.0$)	160.0	61.7	10.5	2.6	15.2	1.5	10.0
	1.0 ($F=0.734$)	199.8	51.6	12.4	3.9	16.2	1.1	5.0
	1.5	26.7	69.2	3.1	0.39	8.6	1.0	6.5

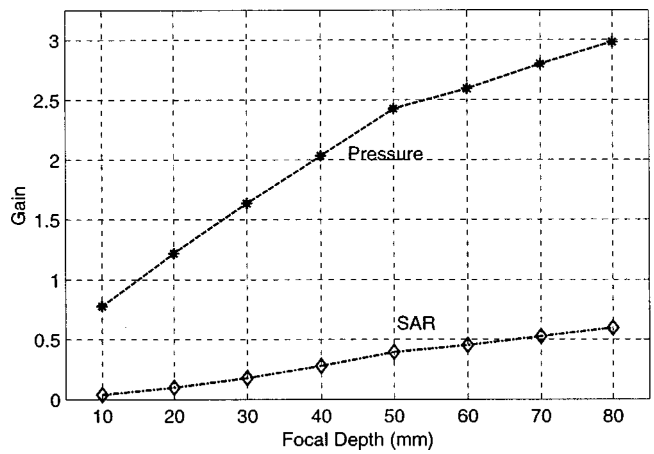

FIG. 10. Pressure/SAR gains versus the focal depth inside the skull.

smallest at 1.5 MHz. Although a lower-frequency enjoys many advantages like lower attenuation in the skull, etc., its applicability is limited by its focal volume size, which calls for a trade-off in practical use.

V. CONCLUSIONS

A numerical model was developed to evaluate acoustic field in multiple layers with irregular layer interface shapes from a spherically curved phased array. This method was applied to evaluating the transskull ultrasound field in the brain. A digitized human skull profile was obtained from MR images which was then used to specify the layer interfaces in the numerical simulations.

Without phase correction, a single transskull focus could be obtained for frequencies below 1.0 MHz, but not for higher frequencies. The phased array technique could be used to restore the destroyed focus, correct focal shift, reduce side lobes, and enhance focal amplitude at all frequencies. The optimum element width for a phased array in order to achieved the near optimum focus was determined to be less 5–6 times the acoustic wavelength. However, due to inevitable skull overheating, frequencies above 1.0 MHz are deemed to be not appropriate for transskull therapy and surgery. The appropriate frequency range for transskull therapy and surgery is below 1.0 MHz which confirms the results previously obtained.[3,4,12] By increasing the skull penetration area, both the pressure and SAR gains can be increased.

Despite high attenuation, complex interface shape, and nonuniform thickness of a human skull, sharply focused transskull ultrasound fields can be generated for noninvasive ultrasound therapy and surgery in the brain.

ACKNOWLEDGMENTS

This research was supported by PHS Grant No. CA 46627 awarded by NCI/NIH, PHHS. The authors would like to thank the reviewers for their comments on the potential difficulties in applying cavitation effects for brain therapy and surgery.

[1] J. G. Lynn, R. L. Zwemer, A. J. Chick, and A. E. Miller, ''A new method for the generation and use of focused ultrasound in experimental biology,'' J. Gen. Physiol. **26**, 179–193 (1942).

[2] W. J. Fry, J. W. Barnard, F. J. Fry, R. F. Krumins, and J. F. Brennan, ''Ultrasonic lesions in the mammalian central nervous system,'' Science **122**, 517–518 (1955).

[3] F. J. Fry, ''Transskull transmission of an intense focused ultrasonic beam,'' Ultrasound Med. Biol. **3**, 179–184 (1977).

[4] F. J. Fry and J. E. Barger, ''Acoustical properties of the human skull,'' J. Acoust. Soc. Am. **63**, 1576–1590 (1978).

[5] J. B. Marmor and G. M. Hahn, ''Ultrasound heating in previously irradiated sites,'' Int. Journal of Radiation Oncology and Biological Physics **4**, 1029–1032 (1978).

[6] F. J. Fry and S. A. Goss, ''Further studies of the transskull transmission of an intense focused ultrasonic beam: Lesion production at 500 kHz,'' Ultrasound Med. Biol. **6**, 33–38 (1980).

[7] P. M. Corry, B. Barlogie, E. J. Tilchen, and E. P. Armour, ''Fundamental results concerning integral representation in acoustical radiation,'' Int. Journal of Radiation Oncology and Biological Physics **8**, 1225–1229 (1982).

[8] F. J. Fry, N. T. Sanghvi, R. F. Morris, S. Smithson, L. Atkinson, K. Dines, T. Franklin, and J. Hastings, ''A focused ultrasound system for tissue volume ablation in deep seated brain sites,'' Proceedings of IEEE 1986 Ultrasonics Symposium **2**, 1001–1004 (1986).

[9] A. N. Guthkelch, L. P. Carter, J. R. Cassady, K. Hynynen, K. Iacono, R. P. Johnson, P. C. Obbens, E. A. Roemer, R. B. Seeger, J. F. Shimm, and B. Stea, ''Treatment of malignant brain tumors with focussed ultrasound hyperthermia and radiation: Results of a phase I trial,'' Journal of Neuro-Oncology **10**, 271–284 (1991).

[10] E. B. Hutchinson, M. T. Buchanan, and K. Hynynen, ''Design and optimization of an aperiodic ultrasound phased array for intracavitary prostate thermal therapies,'' Med. Phys. **23**, 767–776 (1996).

[11] K. M. Quan, D. J. Watmough, and J. R. Mallard, ''Theoretical considerations in relation to the treatment of brain tumours by means of local hyperthermia generated by ultrasound fields,'' European Journal of Surgical Oncology **17**, 454–465 (1991).

[12] K. Hynynen and F. Jolesz, ''Demonstration of noninvasive ultrasound brain therapy through an intact skull,'' Ultrasound Med. Biol. **24**, 275–283 (1998).

[13] S. W. Smith, D. J. Phillips, O. T. von Ramm, and F. L. Thurstone, ''Some advances in acoustic imaging through skull,'' in *Symposium on Biological Effects and Characterizations of Ultrasound Sources*, edited by D. G. Hazzard and M. L. Litz, pp. 37–52 (HEW, Rockville, MD, 1977).

[14] S. W. Smith, G. E. Trahey, and O. T. von Ramm, ''Phased array ultrasound imaging through planar tissue layers,'' Ultrasound Med. Biol. **12**, 229–243 (1986).

[15] J.-L. Thomas and M. A. Fink, ''Ultrasonic beam focusing through tissue inhomogeneities with a time reversal mirror: Application to transskull therapy,'' IEEE Trans. Ultrason. Ferroelectr. Freq. Control **43**, 1122–1129 (1996).

[16] K. Hynynen, A. Chung, T. Fjield, M. Buchanan, D. Daum, V. Colucci, P. Lopath, and F. A. Jolesz, ''Feasibility of using ultrasound phased arrays for MRI monitored noninvasive surgery,'' IEEE Trans. Ultrason. Ferroelectr. Freq. Control **43**, 1043–1052 (1996).

[17] X. Fan and K. Hynynen, ''The effects of curved tissue layers on the power deposition patterns of therapeutic ultrasound beams,'' Med. Phys. **21**, 25–34 (1994).

[18] X. Fan, ''Noninvasive Ultrasound Surgery using Spherically Curved Phased Arrays,'' Ph. D. thesis, Department of Electrical and Computer Engineering, University of Arizona, 1995.

[19] M. C. Junger and D. Feit, *Sound, Structures, and Their Interaction* (Acoustical Society of America, Woodbury, NY, 1993).

[20] X. Fan and K. Hynynen, ''The effects of wave reflection and refraction at soft tissue interfaces during ultrasound hyperthermia treatments,'' J. Acoust. Soc. Am. **91**, 1727–1736 (1992).

[21] M. F. Hamilton, ''Comparison of three transient solutions for the axial pressure in a focused sound beam,'' J. Acoust. Soc. Am. **92**, 527–532 (1992).

[22] K. E. Frøysa, J. N. Tjøtta, and S. Tjøtta, ''Linear propagation of a pulsed sound beam from a plane or focusing source,'' J. Acoust. Soc. Am. **93**, 80–92 (1993).

[23] X. Fan and K. Hynynen, ''A study of various parameters of spherically curved phased array for noninvasive ultrasound surgery,'' Phys. Med. Biol. **41**, 591–608 (1996).

[24] X. Fan and K. Hynynen, ''Ultrasound surgery using multiple sonications—Treatment time considerations,'' Ultrasound Med. Biol. **22**, 471–482 (1996).

[25] P. T. Christopher and K. J. Parker, ''New approaches to the linear propagation of acoustic fields,'' J. Acoust. Soc. Am. **90**, 507–521 (1991).
[26] X. Fan and K. Hynynen, ''Control of the necrosed tissue volume during nonivasive ultrasound surgery using a 16-element phased array,'' Med. Phys. **22**, 297–306 (1995).
[27] K. Hynynen, ''The role of nonlinear ultrasound propagation during hyperthermia treatments,'' Med. Phys. **18**, 1156–1163 (1991).
[28] N. I. Vykhodtseva, K. Hynynen, and C. Damianou, ''Histologic effects of high intensity pulsed ultrasound exposure with subharmonic emission in rabbit brain *in vivo*,'' Ultrasound Med. Biol. **21**, 969–979 (1995).
[29] F. J. Fry, ''Intense focused ultrasound in medicine,'' European Urology **23**, 2–7 (1993).